

Article

# Ethanol Oxidation Reaction on Tandem Pt/Rh/SnO<sub>x</sub> Catalyst

Phuong Tu Mai, Akinori Haze, Masanobu Chiku, Eiji Higuchi and Hiroshi Inoue \*

Department of Applied Chemistry, Graduate School of Engineering, Osaka Prefecture University, Sakai, Osaka 599-8531, Japan; dy105022@edu.osakafu-u.ac.jp (P.T.M.); markedcards3@yahoo.co.jp (A.H.); chiku@chem.osakafu-u.ac.jp (M.C.); e-higuchi@chem.osakafu-u.ac.jp (E.H.)

\* Correspondence: inoue-h@chem.osakafu-u.ac.jp; Tel.: +81-722-254-9283

Received: 18 July 2017; Accepted: 20 August 2017; Published: 24 August 2017

**Abstract:** To elucidate the atomic arrangement of a Pt-Rh-Sn ternary catalyst with a high catalytic activity for ethanol oxidation reaction (EOR) and high CO<sub>2</sub> selectivity, we prepared a tandem Pt/Rh/SnO<sub>x</sub>, in which a Rh adlayer was deposited on a Pt substrate (Rh coverage: 0.28), followed by depositing several layers of SnO<sub>x</sub> only on the Rh surface (Sn coverage: 0.07). For reference, Sn was randomly deposited on the Rh-modified Pt (Pt/Rh) electrode whose Rh and Sn coverages were 0.22 and 0.36 (random Pt/Rh/SnO<sub>x</sub>). X-ray photoelectron spectroscopy demonstrated that Pt and Rh were metallic, and Sn was largely oxidized. Both Pt/Rh/SnO<sub>x</sub> electrodes were less positive in onset potential of EOR current density and higher in EOR current density than Pt and Rh/Pt electrodes. In situ infrared reflection-absorption spectroscopy demonstrated that the tandem Pt/Rh/SnO<sub>x</sub> electrode did not produce acetic acid, but produced CO<sub>2</sub> in contrast to the random Pt/Rh/SnO<sub>x</sub>, suggesting that a tandem arrangement of Pt, Rh and SnO<sub>x</sub>, in which the Pt and SnO<sub>x</sub> sites were separated by the Rh sites, was effective for selective CO<sub>2</sub> production. In the electrostatic electrolysis at 0.5 V vs. RHE, the tandem Pt/Rh/SnO<sub>x</sub> electrode exhibited higher EOR current density than the Pt and Pt/Rh electrodes after 1.5 h.

**Keywords:** ethanol oxidation reaction; direct ethanol fuel cell; tandem catalyst; Pt/Rh/SnO<sub>x</sub>; infrared reflection-absorption spectroscopy; selective CO<sub>2</sub> production

## 1. Introduction

Direct alcohol fuel cells (DAFCs) have been increasingly attractive due to their applications for portable electric devices [1]. Low-molecular weight alcohol fuels such as methanol and ethanol are liquid at normal temperature, in contrast to hydrogen, making them easy to store and transport. Ethanol is nontoxic and has higher specific energy (8.0 kWh kg<sup>-1</sup>) than methanol (6.1 kWh kg<sup>-1</sup>) [2]; moreover, it is a green fuel that can be produced from biomass [3]. Usually, when DAFCs operate, CO<sub>2</sub> is emitted at the anode. However, if bioethanol is used for DAFCs, they can be zero-CO<sub>2</sub> emission power generators.

EOR, which is the anode reaction of direct ethanol fuel cells, is known to be more sluggish than methanol oxidation reaction, and it is hard to break the C-C bond of ethanol molecules in order to form CO<sub>2</sub>. So far, various Pt-based binary catalysts have been reported to improve the EOR activity [4–8], and PtSn alloy and Pt/SnO<sub>x</sub> catalysts were the best anode catalysts for EOR [9–13]. In these catalysts, Pt facilitates the adsorption and dissociation of ethanol, while Sn provides OH species for the oxidation of poisoning intermediates such as CH<sub>x</sub> and CO on Pt [12], which is known as a bi-functional effect. However, the main product was not CO<sub>2</sub>, but acetaldehyde and acetic acid, the partial EOR products, which are unfavorable for the operation of DEFCs. Meanwhile, PtRh catalysts were effective for the C-C bond cleavage or CO<sub>2</sub> formation, although the EOR activity was low [14,15]. In recent years, the combination of Pt, Rh and Sn has been reported to enhance

EOR activity [16–23]. Strasser et al. reported a single-phase Rh-doped Pt-Sn Niggliite mineral phase worked as an active site for EOR [23]. However, the selectivity for CO<sub>2</sub> production was not always improved [21], suggesting that the arrangement of each element at active sites strongly influences selective CO<sub>2</sub> formation. Adzic et al. suggested, based on the density functional theory calculations for a model of RhPt/SnO<sub>2</sub>(110) surface, that Rh and Pt atoms formed an alloy chain bridging a coordinatively unsaturated Sn and a bridged O, and all adsorbates preferred the pure Rh sites except atomic hydrogen, which favored the Rh-Pt hybrid hollow sites, and were oxidized by OH species at the neighboring SnO<sub>2</sub> sites, leading to the formation of CO<sub>2</sub> [17]. From this suggestion and our previous results [13], we deduced that Rh sites should have been arranged to avoid contacting Pt sites with SnO<sub>2</sub> sites for selective CO<sub>2</sub> formation. To verify this hypothesis, in this study, we used a Pt electrode modified partly with the Rh adlayer, and deposited a Sn atomic layer on the Rh surface after adsorbing CO only on the Pt surface by controlling the potential for CO adsorption, which is denoted tandem Pt/Rh/SnO<sub>x</sub> (Figure 1a). For reference, we randomly deposited the Sn atomic layer on the Pt and Rh surface, which is denoted random Pt/Rh/SnO<sub>x</sub> (Figure 1b). Moreover, we demonstrated the selective CO<sub>2</sub> formation on the tandem Pt/Rh/SnO<sub>x</sub> electrode by infrared reflection-absorption spectroscopy (IRAS).

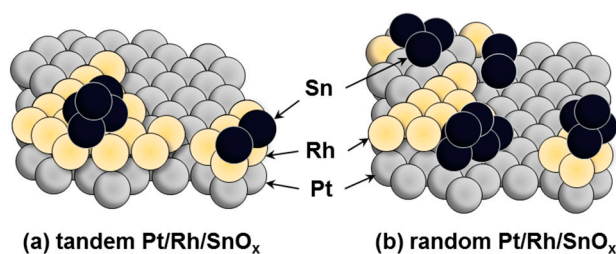


**Figure 1.** Illustrations of (a) tandem Pt/Rh/SnO<sub>x</sub> and (b) random Pt/Rh/SnO<sub>x</sub>.

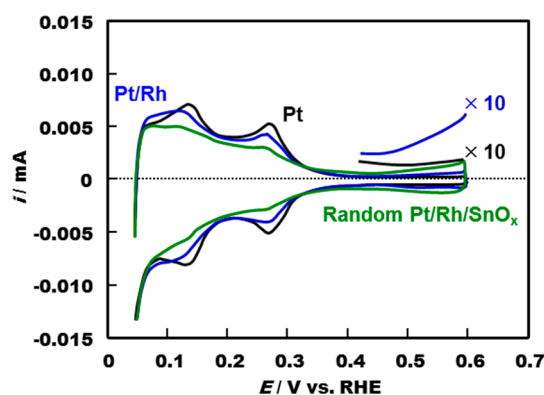
## 2. Results and Discussion

### 2.1. Electrochemical Properties of Pt/Rh and Pt/Rh/SnO<sub>x</sub> Catalysts

Figure 2 shows cyclic voltammograms (CVs) of Pt, Pt/Rh and Pt/Rh/SnO<sub>x</sub> electrodes in an Ar-saturated 0.5 M H<sub>2</sub>SO<sub>4</sub>. For the Pt electrode, two pairs of distinct redox peaks appear around 0.12 and 0.26 V vs. reversible hydrogen electrode (RHE), due to the hydrogen adsorption/desorption at (110) and (100) steps on (111) terraces, respectively [24], which is characteristic of a polycrystalline Pt. After the modification of the Pt surface with the Rh atomic layer, the redox peaks around 0.12 and 0.26 V decreased, whereas the redox peaks around 0.1 V due to hydrogen adsorption/desorption on Rh [25] increased. This suggests that the Rh atoms partially covered both step sites of the Pt surface. It is known that the first Rh adlayer pseudomorphically grows on the terrace surface to form two-dimensional islands [26]. In addition, the increase in current from about 0.5 V vs. RHE can be attributed to the electrochemical formation/reduction of hydroxide on the Rh surface [25]. From the amount of deposited Rh determined by inductively coupled plasma-mass spectroscopy (ICP-MS), the coverage of the Rh atomic layer was estimated to be 0.35, supposing no multilayer was formed.

After the random deposition of Sn on the Pt/Rh electrode, the redox peaks around 0.12 and 0.26 V for Pt and around 0.1 V for Rh were reduced due to the modification of Sn on the Pt/Rh surface, as shown in Figure 2. It is hard to precisely determine the coverage of Sn, because the waves for hydrogen adsorption/desorption on the Pt and Rh surface overlap each other, and they cannot be separated. But Pt and Rh have the same crystal structure and similar lattice parameters, and Rh is pseudomorphically deposited on the Pt surface [26]. So the Sn coverage was roughly estimated from the difference in electric charge of the hydrogen desorption wave between the SnO<sub>x</sub>-modified and unmodified Pt/Rh electrodes, supposing 210 μC cm<sup>-2</sup> [19]. The Sn coverage estimated from Figure 2 was 0.36. When Sn is randomly deposited on the Pt and Rh surface, the coverages of Sn on the Pt and

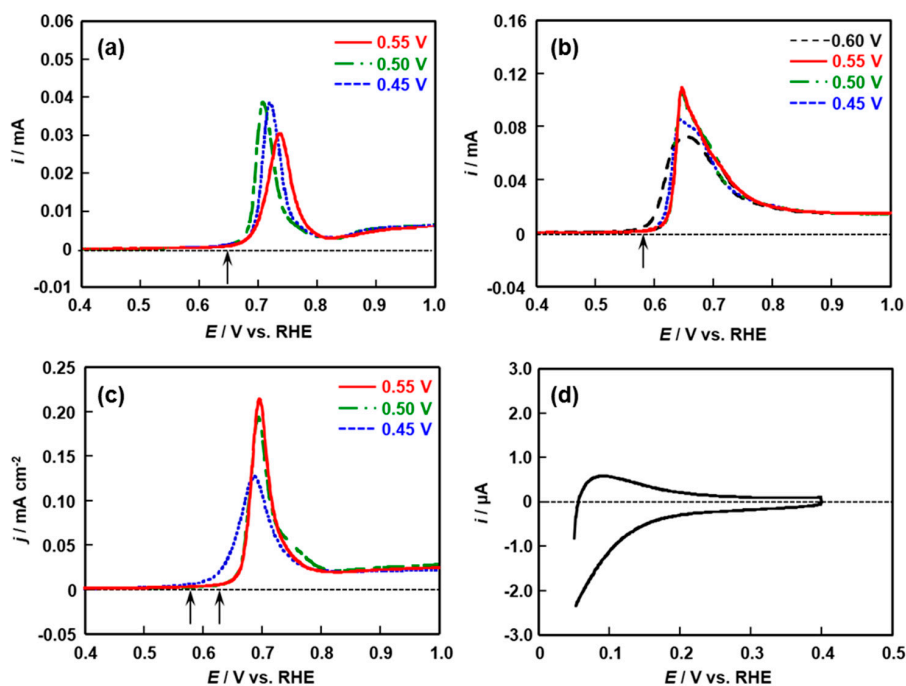
Rh surface are calculated as 0.23 and 0.13, respectively, so the Rh coverage and the fraction of exposed Pt are 0.22 and 0.42, respectively. From the Sn coverage and the amount of deposited Sn determined by ICP-MS, the Sn deposit was estimated to be ca. 4 monolayers in thickness.



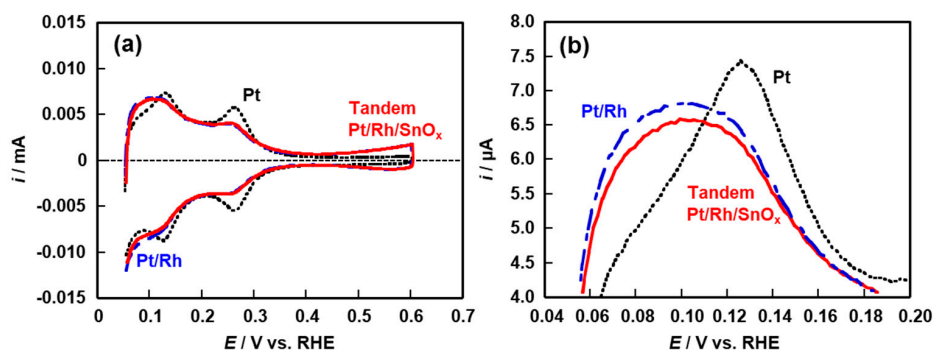
**Figure 2.** Cyclic voltammograms of Pt, Pt/Rh and random Pt/Rh/SnO<sub>x</sub> electrodes in an Ar-saturated 0.5 M H<sub>2</sub>SO<sub>4</sub>. The oxidation current for Pt and Pt/Rh electrodes is partially enlarged tenfold. Sweep rate: 20 mV s<sup>-1</sup>.

To deposit Sn only on the Rh surface, we examined to cover the Pt surface with CO. Figure 3a–c show CO stripping voltammograms of Pt, Rh, and Pt/Rh electrodes in an Ar-saturated 0.1 M HClO<sub>4</sub> solution after CO was adsorbed at 0.45–0.60 V vs. RHE. The onset potentials of CO stripping for the Pt and Rh electrodes were ca. 0.65 and 0.58 V, respectively, irrespective of the potential for CO adsorption ( $E_{ad}$ ) as shown in Figure 3a,b, indicating that CO on Rh was removed more easily than on Pt. For the Pt/Rh electrode, when  $E_{ad}$  was 0.45 V, the onset potential of CO stripping was ca. 0.58 V, which was in agreement with the onset potential of CO stripping on Rh. In contrast, when  $E_{ad}$  was 0.50 or 0.55 V, the onset potential of CO stripping shifted to 0.63 V, which was quite close to the onset potential for CO stripping on Pt. Moreover, when  $E_{ad}$  was 0.60 V, there was no stripping peak, although the CO stripping peak for the Rh electrode was observed even at 0.6 V, as shown in Figure 3b, suggesting that the Rh adlayer for the Pt/Rh electrode was influenced by the underlying Pt, probably through an electronic perturbation [26]. Thus, for the Pt/Rh electrode, at  $E_{ad} = 0.45$  V, CO was adsorbed on both the Rh and Pt surface, whereas at  $E_{ad} = 0.50$  and 0.55 V, CO was adsorbed only on the Pt surface. Moreover, at  $E_{ad} = 0.60$  V, CO was not adsorbed on both Pt and Rh. The CV of the Pt/Rh electrode after the CO adsorption at 0.53 V vs. RHE was shown in Figure 3d. Two couples of redox peaks due to hydrogen adsorption/desorption on Pt disappeared, and the CV was quite similar to that of the Rh electrode, clearly indicating that CO was adsorbed only on the Pt surface to maintain bare Rh surface.

To make a tandem Pt/Rh/SnO<sub>x</sub> electrode, CO was adsorbed on the Pt surface of the Pt/Rh electrode at 0.5 V vs. RHE, and then Sn was deposited on the bare Rh surface by the H-upd method. Figure 4 shows CVs of tandem Pt/Rh/SnO<sub>x</sub> electrode as well as Pt and Pt/Rh electrodes in an Ar-saturated 0.5 M H<sub>2</sub>SO<sub>4</sub>. The two redox peaks due to the hydrogen adsorption/desorption on Pt did not change after the Sn deposition, and the redox peak current due to the hydrogen adsorption/desorption on Rh decreased as shown in Figure 4b, strongly suggesting that Sn was deposited only on the Rh surface. The coverage of Sn was estimated to be 0.07. Therefore, the Pt and Rh coverages of the tandem Pt/Rh/SnO<sub>x</sub> electrode were 0.65 and 0.28, respectively.



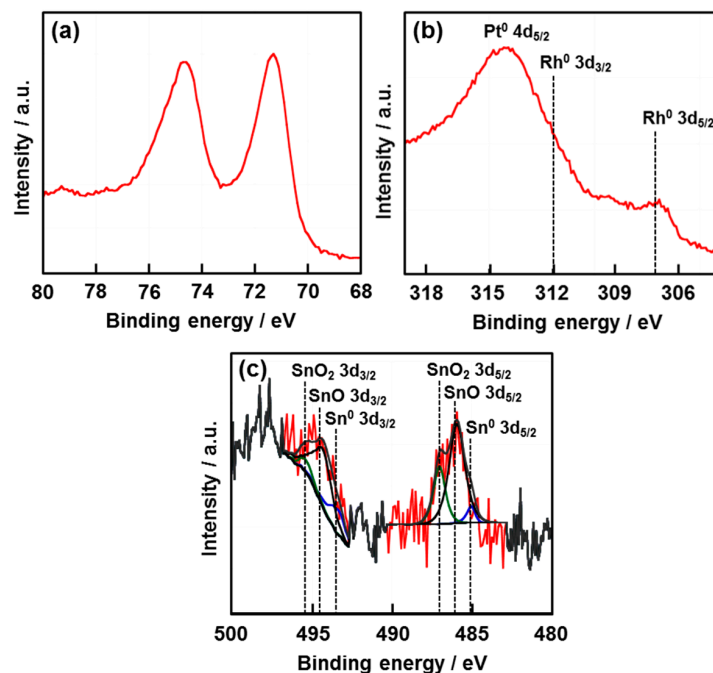
**Figure 3.** CO stripping voltammograms of (a) Pt; (b) Rh and (c) Pt/Rh electrodes after CO was adsorbed at 0.45–0.60 V vs. RHE; and (d) CV of Pt/Rh electrode after Co adsorption at 0.53 V vs. RHE and then CO stripping measurement. Sweep rate:  $20 \text{ mV s}^{-1}$ .



**Figure 4.** (a) CVs and (b) enlarged CVs of tandem Pt/Rh/SnO<sub>x</sub> electrode as well as Pt and Pt/Rh electrodes in an Ar-saturated  $0.5 \text{ M H}_2\text{SO}_4$ . Sweep rate:  $20 \text{ mV s}^{-1}$ .

## 2.2. Electronic State of Each Element for Tandem Pt/Rh/SnO<sub>x</sub> Catalyst

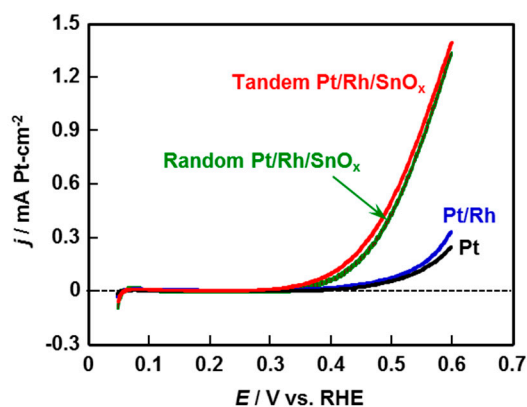
Figure 5 shows Pt4f, Rh3d, and Sn3d core level spectra of tandem Pt/Rh/SnO<sub>x</sub> electrode. In Figure 5a, the doublets at 71.0 and 74.3 eV were assigned to metallic Pt 4f<sub>7/2</sub> and 4f<sub>5/2</sub> [21]. In Figure 5b, the peak for metallic Rh 3d<sub>5/2</sub> was detected at 307.2 eV [21], but the peak for Rh 3d<sub>3/2</sub> at 312 eV was almost hidden by the strong peak for metallic Pt 4d<sub>5/2</sub>. The Sn3d spectrum consisted of overlapped Sn 3d<sub>5/2</sub> and 3d<sub>3/2</sub> doublets assigned to metallic Sn, SnO, and SnO<sub>2</sub> as shown in Figure 5c. The contents of Sn, SnO, and SnO<sub>2</sub> were estimated as 20, 50, and 30 mol %, respectively, indicating that the deposited Sn was mostly oxidized to SnO and SnO<sub>2</sub>, which is named SnO<sub>x</sub> hereafter. These results indicate that the Sn and Rh species on the Pt substrate exist as SnO<sub>x</sub> and metallic Rh.



**Figure 5.** (a) Pt4f; (b) Rh3d and (c) Sn3d core level spectra of tandem Pt/Rh/SnO<sub>x</sub> electrode.

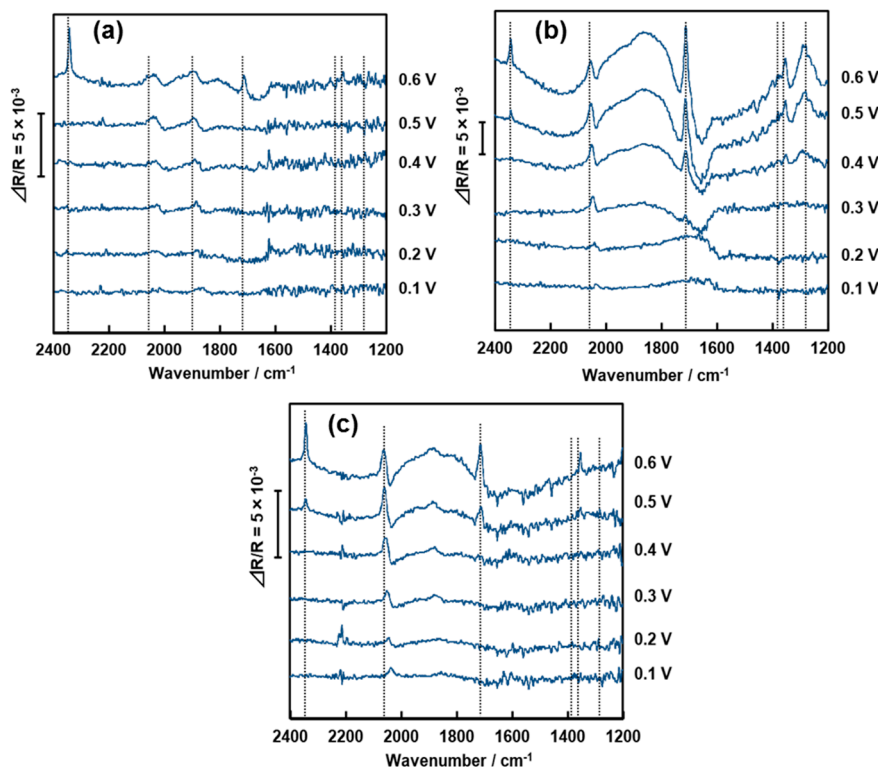
### 2.3. Ethanol Oxidation Reaction Activity and Product Distribution of Pt/Rh and Pt/Rh/SnO<sub>x</sub> Catalysts

Figure 6 illustrates linear sweep voltammograms (LSVs) of Pt, Pt/Rh and random and tandem Pt/Rh/SnO<sub>x</sub> electrodes in an Ar-saturated 0.1 M HClO<sub>4</sub> containing 1 M ethanol. Current density was defined as current per electrochemical surface area of Pt. The onset potential of EOR current density ( $E_{\text{onset}}$ ) for the random and tandem Pt/Rh/SnO<sub>x</sub> electrodes were similar to each other (ca. 0.3 V vs. RHE), which was 0.1 V less positive than that for the Pt and Pt/Rh electrodes (ca. 0.4 V vs. RHE), suggesting that the electrodes containing SnO<sub>x</sub> reduced overpotential for EOR. In addition, the EOR current density at 0.6 V for the random and tandem Pt/Rh/SnO<sub>x</sub> electrodes was nearly 5 times as high as that for the Pt and Pt/Rh electrodes, suggesting that the electrodes containing SnO<sub>x</sub> enhanced the EOR current density due to a synergistic effect of Pt or Rh and Sn [18]. It is known that the adsorbed intermediates formed in EOR on Pt and Rh can be easily oxidized with the supply of O species from SnO<sub>x</sub> adjacent to Pt and Rh, which is the bifunctional mechanism [20]. Thus, in the present study, the enhancement of the EOR current density for both Pt/Rh/SnO<sub>x</sub> electrodes will be attributed to the bifunctional effect between Pt or Rh and SnO<sub>x</sub>.



**Figure 6.** Linear sweep voltammograms of Pt, Pt/Rh and random and tandem Pt/Rh/SnO<sub>x</sub> electrodes in an Ar-saturated 1 M ethanol/0.1 M HClO<sub>4</sub> solution. Sweep rate: 20 mV s<sup>-1</sup>.

To identify EOR intermediates and products, in situ IRAS spectra were measured at various potentials in an Ar-saturated 1 M ethanol/0.1 M HClO<sub>4</sub> solution for Pt/Rh and random and tandem Pt/Rh/SnO<sub>x</sub> electrodes. The results are summarized in Figure 7. For the Pt/Rh electrode, the bands around 2050 [27] and 2016 cm<sup>-1</sup> [28] due to CO linearly bonded on Pt and Rh sites (Pt-CO<sub>L</sub>, Rh-CO<sub>L</sub>), respectively, were observed at 0.2 V and more, as shown in Figure 7a. Each band was also observed for pure Pt or Rh electrode. In addition, the band due to bridged CO (Rh-CO<sub>B</sub>) was observed around 1900 cm<sup>-1</sup> [28], which was also observed for the Rh electrode. The band at 2343 cm<sup>-1</sup> due to the asymmetric stretching mode of CO<sub>2</sub> [18,23] was observed at 0.6 V. CO on Rh sites is probably preferentially oxidized to CO<sub>2</sub>, because CO on Rh was oxidized at less positive potential than that on Pt, as shown in Figure 2. These results suggest that dissociative adsorption and the C-C bond cleavage of ethanol molecules occurred on both Pt and Rh atoms, and CO<sub>2</sub> was formed by the bi-functional effect with OH, which would be formed by activation of water molecules at Pt/Rh step sites [29]. At 0.6 V, a small band due to C=O stretching mode in acetic acid and acetaldehyde, which are partial EOR products, appeared at 1712 cm<sup>-1</sup> [18,23]. The band at 1277 cm<sup>-1</sup> due to the C-O stretching mode of acetic acid and at 1350 and 1390–1410 cm<sup>-1</sup> due to the CH<sub>3</sub> in-plane bending mode and O-C-O stretching of adsorbed acetate [18,23], respectively, were not observed as shown in Figure 7a. Thus, the band at 1712 cm<sup>-1</sup> can be attributed to the formation of acetaldehyde.



**Figure 7.** In situ infrared reflection-absorption spectra at various potentials in an Ar-saturated 1 M ethanol/0.1 M HClO<sub>4</sub> solution for (a) Pt/Rh and (b) random and (c) tandem Pt/Rh/SnO<sub>x</sub> electrodes.

For the random Pt/Rh/SnO<sub>x</sub> electrode, the band at 1712 cm<sup>-1</sup> appeared around 0.3 V, and its intensity greatly increased with potential as shown in Figure 7b. In addition, the band at 1277 cm<sup>-1</sup> due to acetic acid and the band around 1350 cm<sup>-1</sup> due to adsorbed acetate appeared at 0.4 V, and their band intensity also increased with potential. These results suggest that acetic acid and acetate are produced by partial EOR via acetaldehyde. Moreover, the CO<sub>2</sub> production started at 0.5 V, which was ca. 0.1 V less positive than for the Pt/Rh electrode. Adzic et al. reported that for PtSnO<sub>2</sub> catalyst, SnO<sub>2</sub> inhibited ethanol dissociative adsorption on Pt and only facilitated the partial EOR pathway,

whereas RhSnO<sub>2</sub> catalyst improved the C-C bond cleavage, and CO<sub>2</sub> was the major EOR product [20]. For the random Pt/Rh/SnO<sub>x</sub> electrode, SnO<sub>x</sub> is deposited on both Pt and Rh. Thus, in the present study, the partial EOR will mainly occur at the Pt sites adjacent to SnO<sub>x</sub>, whereas the complete EOR will occur at the Rh sites adjacent to SnO<sub>x</sub>. As for CO, only the band due to CO<sub>L</sub> on Pt was observed, because the modification of SnO<sub>x</sub> on Rh reduced the sites for CO adsorption and the modified SnO<sub>x</sub> facilitated the oxidation of CO<sub>B</sub> and CO<sub>L</sub> on Rh.

In situ IRAS spectra for the tandem Pt/Rh/SnO<sub>x</sub> electrode (Figure 7c) exhibited a similar trend to those for the Pt/Rh electrode. The CO<sub>2</sub> production was observed at 0.5 V and more like the random Pt/Rh/SnO<sub>x</sub> electrode, but the band intensity was stronger for the tandem Pt/Rh/SnO<sub>x</sub> electrode. Moreover, the band around 1712 cm<sup>-1</sup> for acetaldehyde greatly reduced, and the band for acetic acid as the end product of partial EOR was not observed even at 0.6 V in contrast to the random Pt/Rh/SnO<sub>x</sub> electrode, because for the tandem Pt/Rh/SnO<sub>x</sub> electrode, SnO<sub>x</sub> was deposited only on Rh, and facilitated the oxidation of CO on Rh adjacent to SnO<sub>x</sub>, which greatly reduced the intensities of Rh-CO<sub>L</sub> and Rh-CO<sub>B</sub> bands. In this sense, one can say that the tandem Pt/Rh/SnO<sub>x</sub> is more appropriate atomic arrangement for selective CO<sub>2</sub> formation than the random one.

#### 2.4. Durability of Pt/Rh and Pt/Rh/SnO<sub>x</sub> Catalysts

Figure 8 shows time courses of EOR current density at 0.5 V vs. RHE for Pt, Pt/Rh and random and tandem Pt/Rh/SnO<sub>x</sub> electrodes in an Ar-saturated 1 M ethanol/0.1 M HClO<sub>4</sub> solution. The random and tandem Pt/Rh/SnO<sub>x</sub> electrodes initially exhibited higher EOR current density than the Pt and Pt/Rh electrodes, as expected from Figure 6. Both Pt/Rh/SnO<sub>x</sub> electrodes exhibited higher EOR current density even after 1.5 h because SnO<sub>x</sub> facilitated the oxidation of intermediate CO. However, CO on Pt was not removed for both Pt/Rh/SnO<sub>x</sub> electrodes as shown in Figure 7b,c, which caused the decay of EOR current density. The optimization of SnO<sub>x</sub> and Rh coverages for the tandem Pt/Rh/SnO<sub>x</sub> electrode will improve the durability as well as the EOR activity and CO<sub>2</sub> selectivity.

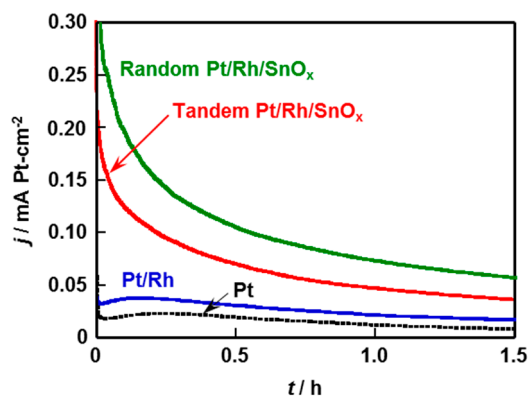


**Figure 8.** Time courses of ethanol oxidation current density at 0.5 V vs. RHE for Pt, Pt/Rh and random and tandem Pt/Rh/SnO<sub>x</sub> electrodes in an Ar-saturated 1 M ethanol/0.1 M HClO<sub>4</sub> solution.

### 3. Experimental

#### 3.1. Preparation of Pt/Rh and Pt/Rh/SnO<sub>x</sub> Catalysts

Rh was deposited on a polycrystalline Pt electrode (diameter: 5 mm) by galvanic replacement with atomic hydrogen pre-adsorbed on the Pt surface, which is named a H-upd method. Briefly, atomic hydrogen was adsorbed on the Pt electrode surface by applying a constant potential of 0.05 V vs. RHE for 15 s in an Ar-saturated 0.5 M H<sub>2</sub>SO<sub>4</sub> aqueous solution. After that, a 0.5 M H<sub>2</sub>SO<sub>4</sub> aqueous solution containing RhCl<sub>3</sub> was quickly added into the electrolyte solution until the concentration of RhCl<sub>3</sub> was

0.05 mM, following by stirring for 40 s. A Rh atomic layer was formed by galvanic replacement of  $\text{Rh}^{3+}$  ions with atomic hydrogens ( $\text{H}_{\text{ad}}$ ) as represented in the following equation.



The resultant Rh atomic layer-modified Pt (Pt/Rh) electrode was thoroughly rinsed by 0.5 M  $\text{H}_2\text{SO}_4$  solution. The Sn atomic layer was also formed on the Pt/Rh electrode by the H-upd method, and a 0.5 M  $\text{H}_2\text{SO}_4$  aqueous solution containing  $\text{SnCl}_2$  was used instead of the  $\text{RhCl}_3$  solution. The Sn atomic layer was immediately oxidized to  $\text{SnO}_x$ , because it was unfortunately exposed in air before the following experiments. The resultant  $\text{SnO}_x$  layer-modified Pt/Rh electrode is called random Pt/Rh/ $\text{SnO}_x$ . To prepare the tandem Pt/Rh/ $\text{SnO}_x$ , before the deposition of Sn, CO was saturated in the electrolyte solution with applying a potential of 0.5 V vs. RHE for 60 s, leading to selective adsorption of CO molecules on the Pt atoms. After removing the dissolved CO in the electrolyte solution by Ar bubbling, Sn was deposited on the exposed Rh surface by the H-upd method.

### 3.2. Characterization of Pt/Rh and Pt/Rh/ $\text{SnO}_x$ Catalysts

The existence and valence of Sn and Rh in the catalysts were analyzed by X-ray photoelectron spectroscopy. ICP-MS was applied for determining the amount of Rh and Sn deposited on the Pt electrode. In-situ IRAS was used for identifying products of EOR at various potentials. The cell was coupled at its bottom with a  $\text{CaF}_2$  prism beveled at  $60^\circ$  from the surface normal. The spectra were recorded with a resolution of  $4 \text{ cm}^{-1}$ . IR spectra were calculated as the difference in reflectance between the sample spectra (0.1 to 0.6 V) and reference spectrum that was recorded at 0.05 V vs. RHE.

### 3.3. Electrochemical Measurements

CV and LSV of each electrode were measured at a sweep rate of  $20 \text{ mV s}^{-1}$  in Ar-saturated 0.5 M  $\text{H}_2\text{SO}_4$  solution and 0.1 M  $\text{HClO}_4$  solution containing 1 M ethanol at  $25^\circ\text{C}$ , respectively. The counter and reference electrodes used in all electrochemical measurements were a Pt sheet and an RHE, respectively. The durability of each catalyst was conducted at 0.5 V for 1.5 h in an Ar-saturated 1 M ethanol/0.1 M  $\text{HClO}_4$  solution.

## 4. Conclusions

We prepared two kinds of Pt/Rh/ $\text{SnO}_x$  electrodes using a Rh adlayer-modified Pt (Pt/Rh) electrode whose Rh coverage was 0.35. The random Pt/Rh/ $\text{SnO}_x$  electrode was prepared by randomly depositing  $\text{SnO}_x$  on the Pt/Rh electrode by the H-upd method, whereas the tandem Pt/Rh/ $\text{SnO}_x$  electrode was prepared by depositing  $\text{SnO}_x$  only on the Rh surface whose Sn and Rh coverages were 0.07 and 0.28, respectively. The CO adsorption on the Pt/Rh electrode at 0.5 V vs. RHE led to selective adsorption of CO only on the Pt surface. In the XPS spectra of the tandem Pt/Rh/ $\text{SnO}_x$  electrode, Pt and Rh was metallic, and Sn was largely oxidized to SnO and  $\text{SnO}_2$ . The  $E_{\text{onset}}$  values for both Pt/Rh/ $\text{SnO}_x$  electrodes were ca. 0.3 V vs. RHE, which were 0.1 V less positive than those for Pt and Rh/Pt electrodes. The EOR current density at 0.6 V for both ternary catalysts were approximately 5 times higher than that for the Pt and Rh/Pt electrodes. In the potentiostatic electrolysis at 0.5 V vs. RHE the tandem Pt/Rh/ $\text{SnO}_x$  electrode exhibited higher EOR current density than Pt and Pt/Rh electrodes even after 1.5 h. These findings clearly indicate that a tandem arrangement of Pt, Rh and  $\text{SnO}_x$ , in which the Pt and  $\text{SnO}_x$  sites were separated by the Rh sites, was effective for high EOR activity and durability. Moreover, in situ IRAS demonstrated that the tandem Pt/Rh/ $\text{SnO}_x$  electrode did not produce acetic acid, but produced  $\text{CO}_2$ , in contrast to the random Pt/Rh/ $\text{SnO}_x$ . This strongly suggests that the tandem Pt/Rh/ $\text{SnO}_x$  electrode was also effective for selective  $\text{CO}_2$  production.

**Author Contributions:** H.I. conceived and designed the experiments; P.T.M., A.H. and E.H. performed the electrochemical and spectroscopic experiments; M.C. and H.I. analyzed the collected results with P.M., A.H. and E.H.; P.T.M. and H.I. wrote the paper and all other co-authors also participated in revising the paper.

**Conflicts of Interest:** The authors declare no conflict of interest. The founding sponsors had no role in the design of the study; in the collection, analyses, or interpretation of data; in the writing of the manuscript, and in the decision to publish the results.

## References

1. Antolini, A. Pt-Ni and Pt-M-Ni (M = Ru, Sn) Anode Catalysts for Low-Temperature Acidic Direct Alcohol Fuel Cells: A Review. *Energies* **2017**, *10*, 42. [[CrossRef](#)]
2. Vigier, F.; Coutanceau, C.; Perrard, A.; Belgsir, E.M.; Lamy, C. Development of anode catalysts for a direct ethanol fuel cell. *J. Appl. Electrochem.* **2004**, *34*, 439–446. [[CrossRef](#)]
3. Zhou, W.J.; Zhou, B.; Li, W.Z.; Zhou, Z.H.; Song, S.Q.; Sun, G.Q.; Xin, Q.; Douvartzides, S.; Goula, M.; Tsiakaras, P. Performance comparison of low-temperature direct alcohol fuel cells with different anode catalysts. *J. Power Sources* **2004**, *126*, 16–22. [[CrossRef](#)]
4. Oliveira Neto, A.; Giz, M.J.; Perez, J.; Ticianelli, E.A.; Gonzalez, E.R. The Electro-oxidation of Ethanol on Pt-Ru and Pt-Mo Particles Supported on High-Surface-Area Carbon. *J. Electrochem. Soc.* **2002**, *149*, A272–A279. [[CrossRef](#)]
5. Zhou, W.J.; Li, W.Z.; Song, S.Q.; Zhou, Z.H.; Jiang, L.H.; Sun, G.Q.; Xin, Q.; Pouliantis, K.; Kontou, S.; Tsiakaras, P. Bi- and tri-metallic Pt-based anode catalysts for direct ethanol fuel cells. *J. Power Sources* **2004**, *131*, 217–223. [[CrossRef](#)]
6. Rodriguez Varela, F.J.; Savadogo, O. Catalytic Activity of Carbon-Supported Electrocatalysts for Direct Ethanol Fuel Cell Applications. *J. Electrochem. Soc.* **2008**, *155*, B618–B624. [[CrossRef](#)]
7. Kepeniene, V.; Tamasaukaite-Tamasuinaite, L.; Jablonskiene, J.; Vaiciuniene, J.; Kondrotas, R.; Juskenas, R.; Norkus, E. Investigation of Graphene Supported Platinum-Cobalt Nanocomposites as Electrocatalysts for Ethanol Oxidation. *J. Electrochem. Soc.* **2014**, *161*, F1354–F1359. [[CrossRef](#)]
8. Zhou, W.; Li, M.; Zhang, L.; Chan, S.H. Supported PtAu catalysts with different nano-structures for ethanol electrooxidation. *Electrochim. Acta* **2014**, *123*, 233–239. [[CrossRef](#)]
9. Lamy, C.; Rousseau, S.; Belgsir, E.M.; Coutanceau, C.; Leger, J.M. Recent progress in the direct ethanol fuel cell: Development of new platinum-tin electrocatalysts. *Electrochim. Acta* **2004**, *49*, 3901–3908. [[CrossRef](#)]
10. Jiang, L.; Sun, G.; Sun, S.; Liu, J.; Tang, S.; Li, H.; Zhou, B.; Xin, Q. Structure and chemical composition of supported Pt–Sn electrocatalysts for ethanol oxidation. *Electrochim. Acta* **2005**, *50*, 5384–5389. [[CrossRef](#)]
11. Jinag, L.; Colmenares, L.; Jusys, Z.; Sun, G.Q.; Behm, R.J. Ethanol electrooxidation on novel carbon supported Pt/SnO<sub>x</sub>/C catalysts with varied Pt:Sn ratio. *Electrochim. Acta* **2007**, *53*, 377–389. [[CrossRef](#)]
12. Ribeiro, J.; dos Anjos, D.M.; Kokoh, K.B.; Coutanceau, C.; Leger, J.-M.; Olivi, P.; de Andrade, A.R.; Tremiliosi-Filho, G. Carbon-supported ternary PtSnIr catalysts for direct ethanol fuel cell. *Electrochim. Acta* **2007**, *52*, 6997–7006. [[CrossRef](#)]
13. Higuchi, E.; Miyata, K.; Takase, T.; Inoue, H. Ethanol oxidation reaction activity of highly dispersed Pt/SnO<sub>2</sub> double nanoparticles on carbon black. *J. Power Sources* **2011**, *196*, 1730–1737. [[CrossRef](#)]
14. De Souza, J.P.I.; Queiroz, S.L.; Bergamaski, K.; Gonzalez, E.R.; Nart, F.C. Electro-Oxidation of Ethanol on Pt, Rh, and PtRh Electrodes. A Study Using DEMS and in-situ FTIR Techniques. *J. Phys. Chem. B* **2002**, *106*, 9825–9830. [[CrossRef](#)]
15. Lima, F.H.B.; Profeti, D.; Lizcano-Valbuena, W.H.; Ticianelli, E.A.; Gonzalez, E.R. Carbon-dispersed Pt-Rh nanoparticles for ethanol electro-oxidation. Effect of the crystallite size and of temperature. *J. Electroanal. Chem.* **2008**, *617*, 121–129. [[CrossRef](#)]
16. Colmati, F.; Antolini, E.; Gonzalez, E.R. Preparation, structural characterization and activity for ethanol oxidation of carbon supported ternary Pt-Sn-Rh catalysts. *J. Alloys Compd.* **2008**, *456*, 264–270. [[CrossRef](#)]
17. Kowal, A.; Li, M.; Shao, M.; Sasaki, K.; Vukmirovic, M.B.; Zhang, J.; Markovic, N.S.; Liu, P.; Frenkel, A.I.; Adzic, R.R. Ternary Pt/Rh/SnO<sub>2</sub> electrocatalysts for oxidizing ethanol to CO<sub>2</sub>. *Nat. Mater.* **2009**, *8*, 325–330. [[CrossRef](#)] [[PubMed](#)]
18. Li, M.; Kowal, A.; Sasaki, K.; Marinkovic, N.; Su, D.; Korach, E.; Liu, P.; Adzic, R.R. Ethanol oxidation on the ternary Pt-Rh-SnO<sub>2</sub>/C electrocatalysts with varied Pt:Rh:Sn ratios. *Electrochim. Acta* **2010**, *55*, 4331–4338. [[CrossRef](#)]

19. Du, W.; Wang, Q.; LaScala, C.A.; Zhang, L.; Su, D.; Frenkel, A.I.; Mathur, V.K.; Teng, X. Ternary PtSnRh-SnO<sub>2</sub> nanoclusters: Synthesis and electroactivity for ethanol oxidation fuel cell reaction. *J. Mater. Chem.* **2011**, *21*, 8887–8892. [[CrossRef](#)]
20. Li, M.; Zhou, W.-P.; Marinkovic, N.S.; Sasaki, K.; Adzic, R.R. The role of rhodium and tin oxide in the platinum-based electrocatalysts for ethanol oxidation to CO<sub>2</sub>. *Electrochim. Acta* **2013**, *104*, 454–461. [[CrossRef](#)]
21. Higuchi, E.; Takase, T.; Chiku, M.; Inoue, H. Preparation of ternary Pt/Rh/SnO<sub>2</sub> anode catalysts for use in direct ethanol fuel cells and their electrocatalytic activity for ethanol oxidation reaction. *J. Power Sources* **2014**, *263*, 280–287. [[CrossRef](#)]
22. De Souza, E.A.; Giz, M.J.; Camara, G.A.; Antolini, E.; Passos, R.R. Ethanol electro-oxidation on partially alloyed Pt–Sn–Rh/C catalysts. *Electrochim. Acta* **2014**, *147*, 483–489. [[CrossRef](#)]
23. Erini, N.; Lopukrakpam, R.; Petkov, V.; Baranova, E.A.; Yang, R.; Teschner, D.; Huang, Y.; Brankovic, S.R.; Strasser, P. Ethanol Electro-Oxidation on Ternary Platinum-Rhodium-Tin Nanocatalysts: Insights in the Atomic 3D Structure of the Active Catalytic Phase. *ACS Catal.* **2014**, *4*, 1859–1867. [[CrossRef](#)]
24. Solla-Gullón, J.; Rodríguez, P.; Herrero, E.; Aldaz, A.; Feliu, J.M. Surface characterization of platinum electrodes. *Phys. Chem. Chem. Phys.* **2008**, *10*, 1359–1373. [[CrossRef](#)] [[PubMed](#)]
25. Jerkiewicz, G.; Borodzinski, J.J. Studies of formation of very thin oxide films on polycrystalline rhodium electrodes: Application of the Mott-Cabrera theory. *Langmuir* **1993**, *9*, 2202–2209. [[CrossRef](#)]
26. Coméz, R.; Feliu, J.M. Rhodium adlayers on Pt(111) monocrystalline surfaces. Electrochemical behavior and electrocatalysis. *Electrochim. Acta* **1998**, *44*, 1191–1205.
27. Vigier, F.; Coutanceau, C.; Hahn, F.; Belgsir, E.M.; Lamy, C. On the mechanism of ethanol electro-oxidation on Pt and PtSn catalysts: Electrochemical and in situ IR reflectance spectroscopy studies. *J. Electroanal. Chem.* **2004**, *563*, 81–89. [[CrossRef](#)]
28. Leung, L.H.; Goodman, D.W. The oxidation of carbon monoxide on Rh(100) under steady state conditions: An FT-IR study. *Catal. Lett.* **1990**, *5*, 353–360. [[CrossRef](#)]
29. Donadio, D.; Ghiringhelli, L.M.; Site, L.D. Autocatalytic and Cooperatively Stabilized Dissociation of Water on a Stepped Platinum Surface. *J. Am. Chem. Soc.* **2012**, *134*, 19217–19222. [[CrossRef](#)] [[PubMed](#)]



© 2017 by the authors. Licensee MDPI, Basel, Switzerland. This article is an open access article distributed under the terms and conditions of the Creative Commons Attribution (CC BY) license (<http://creativecommons.org/licenses/by/4.0/>).